Comparison of performance between bipolar and unipolar double-frequency sinusoidal pulse width modulation in a digitally controlled H-bridge inverter system*

Lei Bo(雷 博)†, Xiao Guo-Chun(肖国春), and Wu Xuan-Lü(吴旋律)

State Key Laboratory of Electrical Insulation and Power Equipment, School of Electrical Engineering, Xi'an Jiaotong University, Xi'an 710049, *China*

(Received 20 October 2012; revised manuscript received 1 November 2012)

By deriving the discrete-time models of a digitally controlled H-bridge inverter system modulated by bipolar sinusoidal pulse width modulation (BSPWM) and unipolar double-frequency sinusoidal pulse width modulation (UDFSPWM) respectively, the performances of the two modulation strategies are analyzed in detail. The circuit parameters, used in this paper, are fixed. When the systems, modulated by BSPWM and UDFSPWM, have the same switching frequency, the stability boundaries of the two systems are the same. However, when the equivalent switching frequencies of the two systems are the same, the BSPWM modulated system is more stable than the UDFSPWM modulated system. In addition, a convenient method of establishing the discrete-time model of piecewise smooth system is presented. Finally, the analytical results are confirmed by circuit simulations and experimental measurements.

Keywords: bipolar sinusoidal pulse width modulation (SPWM), unipolar double-frequency SPWM, H-bridge inverter, discrete-time model

PACS: 05.45.–a, 84.30.Jc, 47.20.Ky **DOI:** 10.1088/1674-1056/22/6/060509

1. Introduction

With the improvement on performance and the reduction in price of digital controller, the digitally controlled high-frequency switching power converter has aroused much interest.[1] In a digitally controlled system, there is a delay of sampling and calculating, so one-step-delay control is often adopted.[2] Owing to the presence of one-step-delay and the switching nonlinearity, the digitally controlled switching power converter system becomes a strongly nonlinear system.[3] Digital sinusoidal pulse width modulation (SPWM) has received increasing attention in different applications in H-bridge inverters for renewable energy systems, ac motor drives and telecommunication systems.[4–6] The modulation strategy will influence the dynamics of the system significantly.[5–7] Thus, the performances of the different modulation schemes in a digitally controlled high-frequency switching power converter should be studied in depth.

The bipolar SPWM (BSPWM) has been widely used in the digitally controlled H-bridge inverter system because of its simple implementation.[6–8] However, the number of output voltage pulses and the frequency of the lowest harmonic voltage, which can also be named equivalent switching frequency, in the unipolar double-frequency SPWM (UDFSPWM) are twice those in the BSPWM with the same switching frequency.[8–11] The advantage of this method is that the filter elements needed are much less due to the fact that the equivalent switching frequency of the output voltage is twice the switching frequency. Therefore, the UDFSPWM facilitates the choice of filter and has better output waveforms.[11,12] Conventionally, the comparison of the performance between BSPWM and UDFSPWM used is based on the FFT analysis,[10,12] which cannot be used to analyze the dynamics of the system and the underlying mechanism. Up to now, by establishing the discrete-time model of the system, the performances of the UDFSPWM and BSPWM have not been studied.

Generally, the discrete-time model of a piece-wise smooth system can be obtained by 'toggling' the topological sequence in one switching period.[13–16] However, in some cases, the topological sequence in one switching period will be changed. This means that the exact discrete-time model of the system can be obtained by analyzing all possible discrete-time models, which are obtained by using the state equation of the corresponding topological sequence. Therefore, a convenient method of establishing the discrete-time model of the piece-wise smooth system is presented in this paper.

The rest of this paper is organized as follows. In Section 2 BSPWM and UDFSPWM in an H-bridge inverter system are outlined. In Section 3, by the presented convenient method of establishing the discrete-time model, the discrete-time models of an H-bridge inverter system, modulated by BSPWM and UDFSPWM, are obtained respectively. In addition, the performances of the two modulation strategies are compared in

*Project supported by the National Natural Science Foundation of China (Grant No. 51277146), the Foundation of Delta Science, Technology, and the Education Development Program for Power Electronics (Grant No. DREG2011003).

†Corresponding author. E-mail: leibo@stu.xjtu.edu.cn

© 2013 Chinese Physical Society and IOP Publishing Ltd

detail in Section 4. Circuit simulations and experimental measurements are shown in Section 5 to illustrate and verify the theoretical results. Finally, some conclusions are given in Section 6.

2. BSPWM and UDFSPWM

The schematic plot of the digital-controlled H-bridge grid-connected inverter is shown in Fig. 1. The inverter is fed by a DC voltage source E. This inverter operates at a fixed switching frequency f_s. Denote the switching period of the system as T_s. An LC-filter and a resistive load are selected. The controller of this system is composed of a load-voltage outer feedback, an inductor-current inner feedback, and a grid-voltage feedforward. As shown in Fig. 1, i_L is the inductor current; v_R is the load voltage; v_{ref}, denoting $V_m \sin(2\pi ft)$, is the reference of the load voltage; k_{in}, k_{out}, k_{pre}, and k_{sat} are the proportional gains of the outer feedback loop, inner feedback loop, feedforward loop, and the saturator, respectively; i_c is the control signal of the PWM modulator. At the beginning of each switching cycle, i_L and v_R are sampled to compute the i_c using the controller. Then, the desired duty cycles of switches S_1 to S_4 are generated.

The digitally controlled BSPWM and UDFSPWM schemes are used in this paper. Figure 2 illustrates the concrete situation by showing the waveforms of the control signal, the triangular signal, and the pulse drive signal of the two modulation schemes.

The four switches (S_1, S_2, S_3, and S_4) are grouped into two pairs (S_1, S_2) and (S_3, S_4). When the modulation scheme is chosen as BSPWM, both of the switch pairs are controlled by d, which is generated by i_c, in a complementary way. However, when UDFSPWM scheme is adopted, one pair of the switches (S_1, S_2) is controlled by d and the other pair (S_3, S_4) is controlled by d^0, which is generated by i_c^0. In Fig. 2, $i_c^0 = -i_c$. d_n and d_n^0 denote the sampled values of d and d^0 at n-th switching period. Due to the intrinsic time delay of the digital-controlled system, the d_n and d_n^0 should be obtained by comparing i_c and i_c^0 with triangular carrier signal in the $(n-1)$-th switching cycle, respectively.

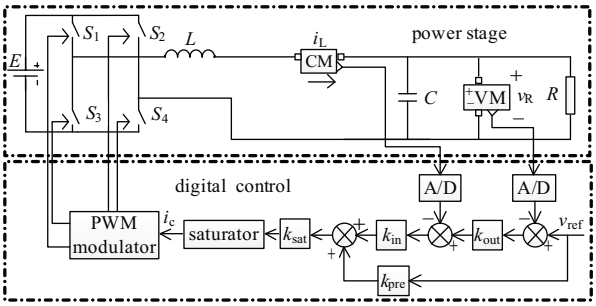


Fig. 1. Digitally controlled H-bridge grid-connected inverter system.

In this kind of modulation scheme, the d_n and d_n^0 can be defined as $d_n = 0.5 + i_c((n-1)T_s)$ and $d_n = 0.5 + i_c^0((n-1)T_s) = 0.5i_c((n-1)T_s)$. For the BSPWM modulated system,

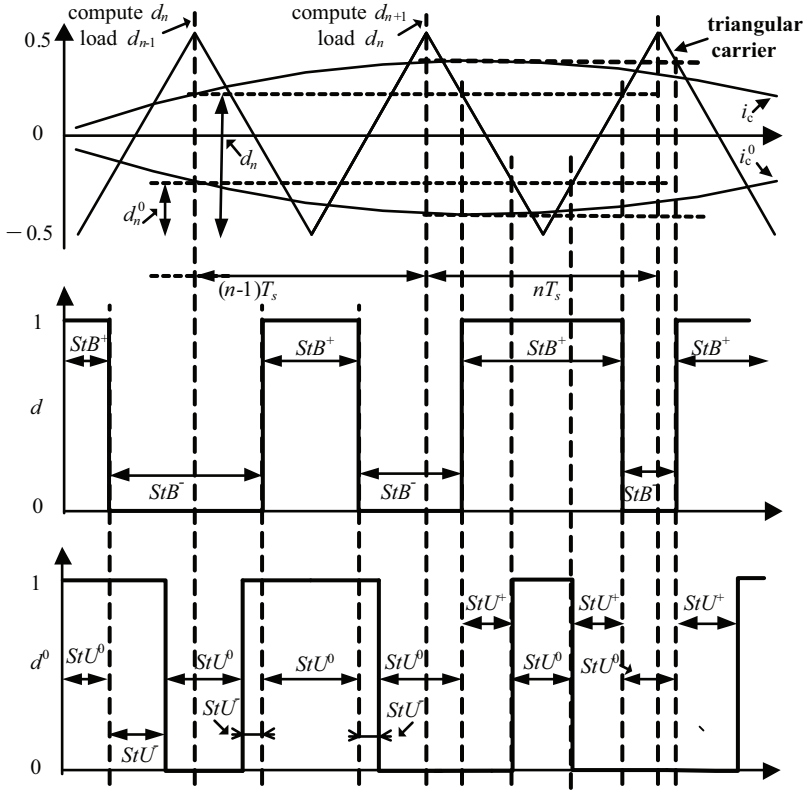


Fig. 2. Waveforms of the control, triangular, and pulse drive signal using BSPWM and UDFSPWM.

when d is "high", the system works in StB^+ state; when d is "low", the system works in StB state. In addition, for the UDFSPWM system when d is "high" and d^0 is "low", the system works in StU^+ state; when d and d^0 are both "high" or "low", the system works in StU state; then, when d is "low" and d^0 is "high", the system works in StU state.

From Figs. 1 and 2, it can be found that the topologies of StB^+ state and StU^+ state are same, while the topologies of StB state and StU state are also the same. Define the state variable vector $\boldsymbol{x} = [i_{\rm L},\ v_{\rm R}]^{\rm T}$. The dynamic behaviors of this H-bridge inverter modulated by BSPWM and UDFSPWM can be described by the following equations:

StB^+ and StU^+ state:

$$\frac{{\rm d}\boldsymbol{x}}{{\rm d}t} = \boldsymbol{A}\boldsymbol{x} + \boldsymbol{B}^+ E; \tag{1a}$$

StB^+ and StU^+ state:

$$\frac{{\rm d}\boldsymbol{x}}{{\rm d}t} = \boldsymbol{A}\boldsymbol{x} + \boldsymbol{B}^- E; \tag{1b}$$

StU state:

$$\frac{{\rm d}\boldsymbol{x}}{{\rm d}t} = \boldsymbol{A}\boldsymbol{x} + \boldsymbol{B}^0 E, \tag{1c}$$

where, $\boldsymbol{A}$, $\boldsymbol{B}^+$, $\boldsymbol{B}$, and $\boldsymbol{B}^0$ are the system matrixes, whose definitions are shown in Appendix A.

From Fig. 2, it can be found that the topology sequence at n-th switching period of the BSPWM modulated system is $StB \to StB^+ \to StB$; the topology sequence of the UDFSPWM modulated system can be $StU \to StU^+ \to StU \to StU^+ \to StU$ (if d is greater than d^0, this situation is defined as US_1) and $StU \to StU \to StU \to StU \to StU$ (if d^0 is greater than d, this situation is defined as US_2). In the following section, the performances of the BSPWM and UDFSPWM in this H-bridge system will be compared with each other in detail by establishing the discrete-time model.

3. Discrete-time model

The system can be divided into power stage block and control block. Owing to the time delay problem and the sampling and holding process, the discrete-time model of control block can be obtained directly, while, the discrete-time model of the power stage block can be derived from the state equations (1a)–(1c). Combining the discrete-time models of the two blocks, the discrete-time model of the whole system can be obtained.

Owing to the presence of the $v_{\rm ref}$ (it is time varying with the line frequency), the accuracy of the discrete-time model depends on the process of "quasi-static" approximation.[17] The reference load voltage at n-th switching period can be written as

$$v_{{\rm ref}n} = v_{\rm ref}(nT_{\rm s}). \tag{2}$$

Define $\boldsymbol{x}$ and d as the state variables. Let $\boldsymbol{x}_n$ d_n, and d_n^0 be the sampled values of $\boldsymbol{x}$ and d at $nT_{\rm s}$, respectively.

3.1. Convenient method of establishing the discrete-time model

Traditionally, the discrete-time model of a piece-wise smooth system can be obtained by 'toggling' the topological sequence in one switching period. It will be complicated when the topology sequence of the system has more than one possibility situation, just like the situation in the H-bridge inverter system modulated by UDFSPWM.

Using the automatic control theory, the dynamics of a system under a motivation can be composed of zero-input response and zero-state response. For one topology in a piece-wise smooth system, the dynamic of this topology is determined by a zero-input response, whose initial state can be obtained by the state of the previous topology, and a zero-state response, whose input is determined by the input in this topology. Suppose that the system has M topology changing in a switching period, the action time of each topology is at t_1–t_M and the response of each topology is $\varphi_1(t_1) - \varphi_M(t_M)$. Since the system matrix $\boldsymbol{A}$ is fixed at different topologies in this system, state-transition matrix can be set as

$$\phi(t) = {\rm e}^{\boldsymbol{A}t}. \tag{3}$$

According to Eq. (1), $\varphi^+(t)$, $\varphi^-(t)$, and $\varphi^0(t)$ can be described as

$$\varphi^+(t) = E(\varphi(t) - \boldsymbol{I})\boldsymbol{A}^{-1}\boldsymbol{B}^+, \tag{4a}$$

$$\varphi^-(t) = E(\varphi(t) - \boldsymbol{I})\boldsymbol{A}^{-1}\boldsymbol{B}^-, \tag{4b}$$

$$\varphi^0(t) = E(\varphi(t) - \boldsymbol{I})\boldsymbol{A}^{-1}\boldsymbol{B}^0 = 0. \tag{4c}$$

The discrete-time model of the system can be described as

$$\boldsymbol{x}_{n+1} = \boldsymbol{x}_n \prod_{j=1}^{M} \phi(t_j) + \sum_{i=1}^{M} \left(\varphi_i(t_i) \prod_{j=M-i}^{M} \phi(t_j) \right). \tag{5}$$

By using Eqs. (3)–(5), the discrete-time model of a piece-wise smooth system can be obtained directly. In addition, when the topology sequence has more than one condition, the difference between the conditions can be analyzed simply.

In one switching period, each special topology spends a fraction of $T_{\rm s}$. Set the beginning and terminative time of one of the topologies to be $t_{\rm on}$ and $t_{\rm off}$ and define $\boldsymbol{x}_{t_{\rm on}}$ and $\boldsymbol{x}_{t_{\rm off}}$ as the sampled values of $\boldsymbol{x}$ at $t_{\rm on}$ and $t_{\rm off}$ respectively, then the discrete-time model of this topology can be given as

$$\begin{aligned} \boldsymbol{x}_{t_{\rm off}} &= \int_{t_{\rm on}}^{t_{\rm off}} (\boldsymbol{A}\boldsymbol{x} + \boldsymbol{B}^{\rm s} E)\,{\rm d}\tau \\ &= \phi(t_{\rm off} - t_{\rm on})\,\boldsymbol{x}_{t_{\rm on}} + \varphi^{\rm s}(t_{\rm off} - t_{\rm on}), \end{aligned} \tag{6}$$

where, $\varphi^{\rm s}$ is the response of this special topology, and $\boldsymbol{I}$ is a second-order unit matrix.

3.2. Discrete-time model of control block

When digitally controlled modulation is applied, d_{n+1} should be determined by $\boldsymbol{x}_n$ and can be determined by:

$$\begin{aligned} d_{n+1} &= 0.5 + k_{\text{sat}}\left(v_{\text{off}n} + k_{\text{in}}\left(k_{\text{out}}\left(v_{\text{off}n} - v_R\right) - i_L\right)\right) \\ &= 0.5 + k_{\text{sat}}\left(1 + k_{\text{in}}k_{\text{out}}\right)v_{\text{off}\,n} \\ &\quad - k_{\text{sat}}k_{\text{in}}i_L - k_{\text{sat}}k_{\text{in}}k_{\text{out}}v_R. \end{aligned} \tag{7}$$

Then, according to Fig. 2, the relationship between d_n and d_n^0 can be described as

$$d_n + d_n^o = 1. \tag{8}$$

3.3. Discrete-time model of power stage block

3.3.1. BSPWM system

In the BSPWM system, the topology sequence is fixed. In the n-th switching period, the action times of $StB-$, StB^+, and StB are $(1-d_n)T_s/2$, d_nT_s, and $(1-d_n)T_s/2$, respectively. Using the conclusion presented in Subsection 3.1, the discrete-time model of power stage block in the H-bridge inverter system modulated by BSPWM can be obtained by

$$\begin{aligned} \boldsymbol{x}_{n+1} &= \phi\left(T_s\right)\boldsymbol{x}_n + E(\phi\left(T_s(1+d_n)/2\right)\varphi^-\left(T_s(1-d_n)/2\right) \\ &\quad + \phi\left(T_s(1-d_n)/2\right)\varphi^+\left(T_sd_n\right) \\ &\quad + \varphi^-(T_s(1-d_n)/2)). \end{aligned} \tag{9}$$

By using the method presented in Ref. [14], equation (9) can be described as:

$$\begin{aligned} i_{\text{L}(n+1)} &= \sigma(1,1,1)i_{\text{L}n} + \sigma(1,1,2)v_{\text{R}n} \\ &\quad + 2E(\Gamma(1,1)(2\sinh(d_n\lambda_{\boldsymbol{A}1}/2) - \sinh(\lambda_{\boldsymbol{A}1}/2)) \\ &\quad + \Gamma(1,2)(2\sinh(d_n\lambda_{\boldsymbol{A}2}/2) - \sinh(\lambda_{\boldsymbol{A}2}/2)), \end{aligned} \tag{10a}$$

$$\begin{aligned} v_{\text{R}(n+1)} &= \sigma(1,2,1)i_{\text{L}n} + \sigma(1,2,2)v_{\text{R}n} \\ &\quad + 2E(\Gamma(2,1)(2\sinh(d_n\lambda_{\boldsymbol{A}1}/2) - \sinh(\lambda_{\boldsymbol{A}1}/2)) \\ &\quad + \Gamma(2,2)(2\sinh(d_n\lambda_{\boldsymbol{A}2}/2) - \sinh(\lambda_{\boldsymbol{A}2}/2)), \end{aligned} \tag{10b}$$

where $\lambda_{\boldsymbol{A}1}$ and $\lambda_{\boldsymbol{A}}$ are the eigenvalues of $\boldsymbol{A}$, the definitions of $\sigma(x, y, z)$ and $\Gamma(x, y)$ are shown in Appendix B.

3.3.2. UDFSPWM system

In the UDFSPWM system, the topology sequence has two possibilities. In the n-th switching period, when the system is in US_1, the action times of StU^0, StU^+, StU^0, StU^+, and StU are $(1-d_n)T_s/2$, $(d_nd_n^0)T_s/2$, d_nT_s, $(d_nd_n^0)T_s/2$, and $(1-d_n)T_s/2$, respectively; when the system is in US_2, the action times of StU^0, StU^-, StU^0, StU, and StU are $(1-d_n^0)T_s/2$, $(d_n^0d_n)T_s/2$, $d_n^0T_s$, $(d_n^0d_n)T_s/2$, and $(1-d_n^0)T_s/2$, respectively. Using the conclusion presented in Subsection 3.1 and Eq. (8), the discrete-time models of power stage block in US_1 and US_2 can be obtained by

for US_1 state

$$\begin{aligned} \boldsymbol{x}_{n+1} &= \phi(T_s)\boldsymbol{x}_n + E(\phi(T_s(1+d_n)/2)\varphi^0(T_s(1-d_n)/2) \\ &\quad + \phi(T_s(1+d_n^0)/2)\varphi^+(T_s(d_n-d_n^o)/2) \\ &\quad + \phi(T_s(1-d_n^0)/2)\varphi^0(T_sd_n^o) \\ &\quad + \phi(T_s(1-d_n)/2)\varphi^+(T_s(d_n-d_n^o)/2) \\ &\quad + \varphi^0(T_s(1-d_n)/2)) \\ &= \phi(T_s)\boldsymbol{x}_n + E(\phi(T_s(1+d_n^0)/2)\varphi^+(T_s(d_n-d_n^o)/2) \\ &\quad + \phi(T_s(1-d_n)/2)\varphi^+(T_s(d_n-d_n^o)/2)); \end{aligned} \tag{11a}$$

for US_2 state,

$$\begin{aligned} \boldsymbol{x}_{n+1} &= \phi(T_s)\boldsymbol{x}_n + E(\phi(T_s(1+d_n^0)/2)\varphi^0(T_s(1-d_n^0)/2) \\ &\quad + \phi(T_s(1+d_n)/2)\varphi^-(T_s(d_n^o-d_n)/2) \\ &\quad + \phi(T_s(1-d_n)/2)\varphi^0(T_sd_n) \\ &\quad + \phi(T_s(1-d_n^0)/2)\varphi^-(T_s(d_n^0-d_n)/2) \\ &\quad + \varphi^0(T_s(1-d_n^0)/2)) \\ &= \phi(T_s)\boldsymbol{x}_n + E(\phi(T_s(1+d_n)/2)\varphi^-(T_s(d_n^0-d_n)/2) \\ &\quad + \phi(T_s(1-d_n^0)/2)\varphi^-(T_s(d_n^0-d_n)/2)). \end{aligned} \tag{11b}$$

By using Eqs. (3) and (4), equations (10a) and (10b) are the same. Therefore, in the subsequent discussions of this paper, equation (10a) will be used as the discrete-time of power stage in the H-bridge inverter system modulated by UDFSPWM.

Similarly, by using the method presented in Ref. [14], equation (11) can be described as

$$\begin{aligned} i_{\text{L}(n+1)} &= \sigma(1,1,1)i_{\text{L}n} + \sigma(1,1,2)v_{\text{R}n} \\ &\quad + E(\Gamma(1,1)(\sinh(d_n\lambda_{\boldsymbol{A}1}2) \\ &\quad + \sinh((d_n-1)\lambda_{\boldsymbol{A}1}/2)) + \Gamma(1,2)(\sinh(d_n\lambda_{\boldsymbol{A}2}/2) \\ &\quad + \sinh((d_n-1)\lambda_{\boldsymbol{A}2}/2))), \end{aligned} \tag{12a}$$

$$\begin{aligned} v_{\text{R}(n+1)} &= \sigma(1,2,1)i_{\text{L}n} + \sigma(1,2,2)v_{\text{R}n} \\ &\quad + E(\Gamma(2,1)(\sinh(d_n\lambda_{\boldsymbol{A}1}/2) \\ &\quad + \sinh((d_n-1)\lambda_{\boldsymbol{A}1}/2)) + \Gamma(2,2)(\sinh(d_n\lambda_{\boldsymbol{A}2}/2) \\ &\quad + \sinh((d_n-1)\lambda_{\boldsymbol{A}2}/2))). \end{aligned} \tag{12b}$$

4. Dynamics analysis of BSPWM and UDFSPWM

Based on the "quasi-static" approximation,[17] there are N_{eq} ($N_{\text{eq}} = f_s/f$) equilibrium points in one line period. By analyzing the N_{eq} equilibrium points, the dynamics of the system can be obtained.

For each switching period, by letting $\boldsymbol{x}_{n+1} = \boldsymbol{x}_n$ and $d_{n+1} = d_n$, the equilibrium point of this switching period can be obtained. Moreover, the dynamics of this switching period can be obtained with the help of the corresponding Jacobian matrix.

$i_{\rm L}^*$, $v_{\rm R}^*$, and d_n^* denote one of the $N_{\rm eq}$ equilibrium points. Define $\boldsymbol{J}_{\rm B}$ and $\boldsymbol{J}_{\rm U}$ as the Jacobian matrixes of the system modulated by BSPWM and UDFSPWM respectively. Also $\boldsymbol{J}_{\rm B}$ and $\boldsymbol{J}_{\rm U}$ can be described as:

$$\boldsymbol{J}_{\rm B} = \begin{bmatrix} \sigma(1,1,1) & \sigma(1,1,2) & \Lambda_{\rm B1} \\ \sigma(1,2,1) & \sigma(1,2,2) & \Lambda_{\rm B2} \\ -k_{\rm sat}k_{\rm in} & -k_{\rm sat}k_{\rm in}k_{\rm out} & 0 \end{bmatrix}_{\boldsymbol{x}_n=\boldsymbol{x}_n^*;d_n=d_n^*}, \quad (13a)$$

$$\boldsymbol{J}_{\rm U} = \begin{bmatrix} \sigma(1,1,1) & \sigma(1,1,2) & \Lambda_{\rm U1} \\ \sigma(1,2,1) & \sigma(1,2,2) & \Lambda_{\rm U2} \\ -k_{\rm sat}k_{\rm in} & -k_{\rm sat}k_{\rm in}k_{\rm out} & 0 \end{bmatrix}_{\boldsymbol{x}_n=\boldsymbol{x}_n^*;d_n=d_n^*}, \quad (13b)$$

where $\Lambda_{\rm B1}$, $\Lambda_{\rm B2}$, $\Lambda_{\rm U1}$, and $\Lambda_{\rm U2}$ can be obtained as

$$\begin{aligned}\Lambda_{\rm B1} &= 2E(\Gamma(1,1)\lambda_{\boldsymbol{A}1}\cosh(d_n\lambda_{\boldsymbol{A}1}/2) \\ &\quad + \Gamma(1,2)\lambda_{\boldsymbol{A}2}\cosh(d_n\lambda_{\boldsymbol{A}2}/2)), \quad (14a)\\ \Lambda_{\rm B2} &= 2E(\Gamma(2,1)\lambda_{\boldsymbol{A}1}\cosh(d_n\lambda_{\boldsymbol{A}1}/2) \\ &\quad + \Gamma(2,2)\lambda_{\boldsymbol{A}2}\cosh(d_n\lambda_{\boldsymbol{A}2}/2)), \quad (14b)\\ \Lambda_{\rm U2} &= E(\Gamma(1,1)\lambda_{\boldsymbol{A}1}(\cosh(d_n\lambda_{\boldsymbol{A}1}/2) \\ &\quad + \cosh((d_n-1)\lambda_{\boldsymbol{A}1}/2)) \\ &\quad + \Gamma(1,2)\lambda_{\boldsymbol{A}2}(\cosh(d_n\lambda_{\boldsymbol{A}2}/2) \\ &\quad + \cosh((d_n-1)\lambda_{\boldsymbol{A}2}/2))), \quad (14c)\\ \Lambda_{\rm U2} &= E(\Gamma(2,1)\lambda_{\boldsymbol{A}1}(\cosh(d_n\lambda_{\boldsymbol{A}1}/2) \\ &\quad + \cosh((d_n-1)\lambda_{\boldsymbol{A}1}/2)) \\ &\quad + \Gamma(2,2)\lambda_{\boldsymbol{A}2}(\cosh(d_n\lambda_{\boldsymbol{A}2}/2) \\ &\quad + \cosh((d_n-1)\lambda_{\boldsymbol{A}2}/2))). \quad (14d)\end{aligned}$$

Since the switching frequency is greater than line frequency, so that $d_n\lambda_{A1}/2 \ll 1$, $d_n\lambda_{A2}/2 \ll 1$, $(d_n-1)\lambda_{A1}/2 \ll 1$, and $(d_n-1)\lambda_{A2}/2 \ll 1$. Combined with the definition of function cosh, equations (14) can be simplified, respectively, into

$$\begin{aligned}\Lambda_{\rm B1} &= 2E(\Gamma(1,1)\lambda_{\boldsymbol{A}1}+\Gamma(1,2)\lambda_{\boldsymbol{A}2}), \quad (15a)\\ \Lambda_{\rm B2} &= 2E(\Gamma(2,1)\lambda_{\boldsymbol{A}1}+\Gamma(2,2)\lambda_{\boldsymbol{A}2}), \quad (15b)\\ \Lambda_{\rm U2} &= 2E(\Gamma(1,1)\lambda_{\boldsymbol{A}1}..+\Gamma(1,2)\lambda_{\boldsymbol{A}2}), \quad (15c)\\ \Lambda_{\rm U2} &= 2E(\Gamma(2,1)\lambda_{\boldsymbol{A}1}..+\Gamma(2,2)\lambda_{\boldsymbol{A}2}). \quad (15d)\end{aligned}$$

According to Eqs. (13)–(15), since $\boldsymbol{J}_{\rm B}$ and $\boldsymbol{J}_{\rm U}$ are independent of $\boldsymbol{x}_n^*$ and d_n^*, the dynamic behaviors for all the switching period at one line period are almost the same. In addition, from Eq. (15), it can be found that $\Lambda_{\rm B1}=\Lambda_{\rm U1}$ and $\Lambda_{\rm B2}=\Lambda_{\rm U2}$. Set $\Lambda_1=\Lambda_{\rm B1}=\Lambda_{\rm U1}$, $\Lambda_2=\Lambda_{\rm B2}=\Lambda_{\rm U2}$, then $\boldsymbol{J}_{\rm B}$ and $\boldsymbol{J}_{\rm U}$ will be the same. For this reason, when the systems, modulated by BSPWM and UDFSPWM, have the same switching frequency and circuit parameters, the stability boundaries of the two systems are the same.

Define $\lambda_{\boldsymbol{J}1}$–$\lambda_{\boldsymbol{J}3}$ as the characteristic roots of the Jacobian matrix. By using Eq. (13), the characteristic equation can be written as

$$\lambda_{\boldsymbol{J}}^3+\lambda_{\boldsymbol{J}}^2F_2+\lambda_{\boldsymbol{J}}F_1+F_0=0, \quad (16)$$

where F_0, F_1, and F_2 are coefficients of the characteristic equation, and their definitions are indicated in Appendix C.

Using the conclusion predicted in Refs. [13] and [14], the stability boundary derived by Eq. (16) can be obtained as

$$k_{\rm in} < \frac{\gamma_1}{\gamma_2+\gamma_3 k_{\rm out}}. \quad (17)$$

The definitions of γ_1, γ_2, and γ_3 are given in Appendix C.

Using inequality (17) and the circuit parameters listed in Table 1, two stability boundaries, whose switching frequencies are 10 kHz and 5 kHz respectively, are derived (Fig. 3) to analyze the stabilities of the BSPWM and UDFSPWM-modulated system using the same equivalent switching frequency.

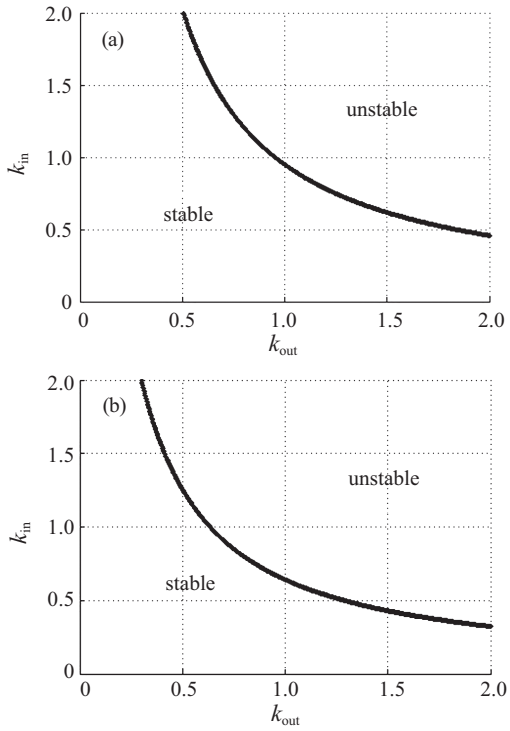


Fig. 3. Stability boundaries with switching frequency $f_{\rm s}=10$ kHz (a) and 5 kHz (b).

From Fig. 3, when $f_{\rm s}=5$ kHz, the equivalent switching frequency of UDFSPWM is 10 kHz, the stability boundary, shown by Fig. 3(b), is smaller than that in Fig. 3(a), whose switching frequency is 10 kHz.

Table 1. Circuit parameters.

Parameters	Value	Parameters	Value
E	100 V	f	50 Hz
L	1 mH	$f_{\rm s}$	5 kHz–10 kHz
C	20 μF	$T_{\rm s}$	0.0002 s–0.0001 s
R	8 Ω	$k_{\rm pre}$	1
$V_{\rm m}$	70	$k_{\rm sat}$	$1/(2E)$=0.005

By using inequality (17), when $f_{\rm s}=10$ kHz, one of the bifurcation points is obtained: $k_{\rm out}=1$ and $k_{\rm out}=0.95$; when the equivalent switching frequency of UDFSPWM system is 10 kHz, one of the bifurcation points is $k_{\rm out}=1$ and $k_{\rm in}=0.68$.

5. Circuit simulation and experiments

In this section, the theoretical results will be verified using circuit simulation and experimental measurements. The circuit parameters, used in this section, are the same as those in Table 1.

According to Fig. 1, the SIMULINK model of the system is shown in Fig. 4. Since there is a power stage, the SIMULINK model is set as 'continuous mode'. Meanwhile, the 'sample time' in the unit-delay and sum module is set as T_s to simulate the time delay and the sampling and holding process. In addition, the BSPWM and UDFSPWM scheme used in simulation are shown in Fig. 5.

The experimental platform of the system is designed according to Fig. 1. IGBTs are used as the switches S_1–S_4 in the inverter. The current and voltage transducer are LEM, LV55-P, and LEM, LV28-P respectively. Additionally, the digital oscilloscope Tektronix DPO3034 is employed to capture the measured waveforms.

When $f_s = 10$ kHz, figures 6 and 7 are shown to verify the conclusion that the systems modulated by BSPWM and UDFSPWM have the same stability boundary when the circuit parameters are the same. k_{out} is chosen to be 1 while k_{in} is chosen to be 0.9 in Fig. 6 and 1 in Fig. 7. In addition, the accuracy of inequality (17) is verified.

When $f_s = 5$ kHz, using $k_{out} = 1$ and $k_{in} = 0.75$, the circuit simulations and experimental measurements of the UDFSPWM modulated system are shown in Fig. 8.

From Fig. 8, it can be found that the system is unstable. The conclusion, i.e., the BSPWM modulated system is more stable than the UDFSPWM when the equivalent switching frequencies of the two systems are the same, is proved.

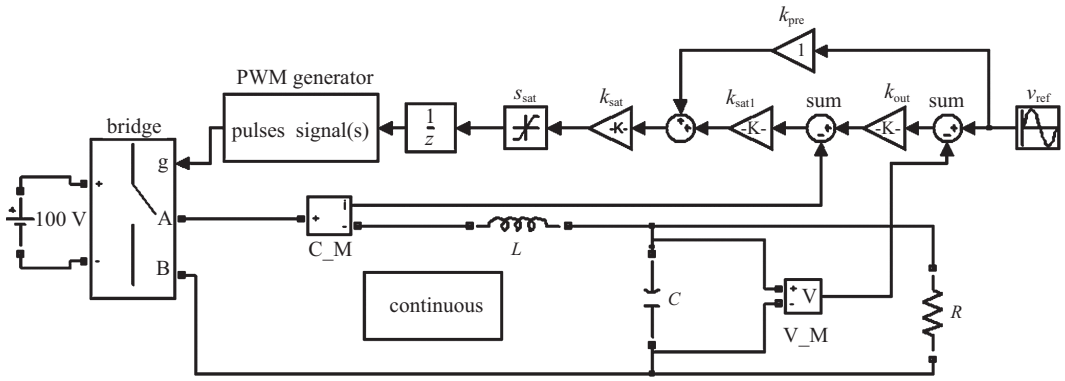
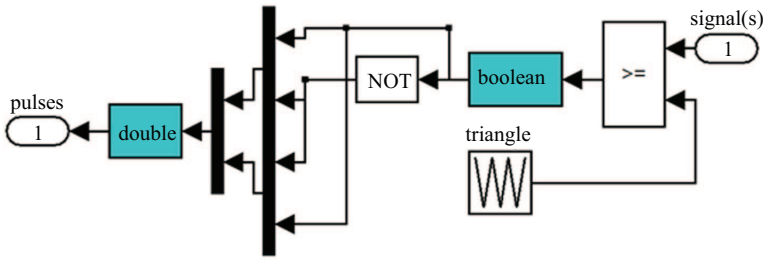
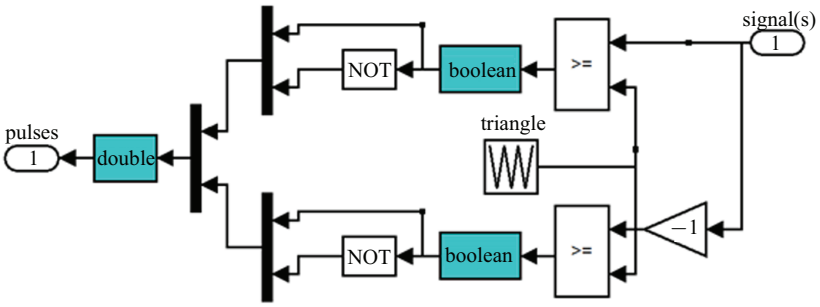


Fig. 4. SIMULINK model of digital-controlled H-bridge inverter system.

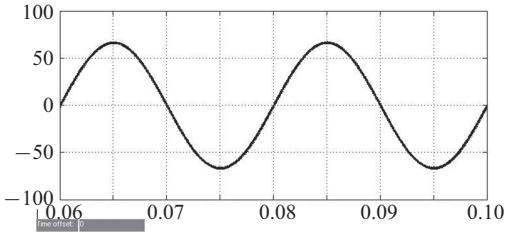


(a) BSPWM scheme

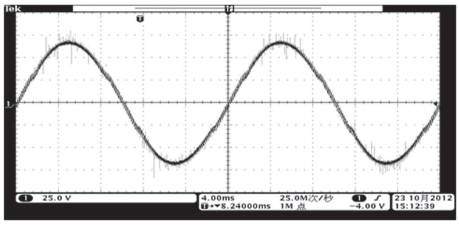


(b) UDFSPWM scheme

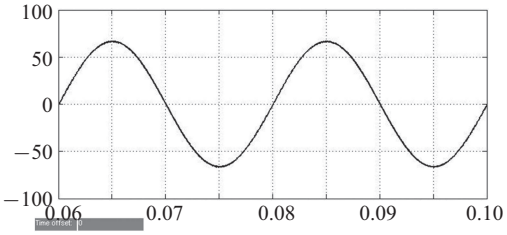
Fig. 5. (color online) BSPWM and UDFSPWM scheme.



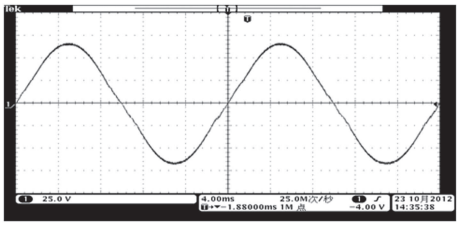
(a) Simulation result of BSPWM system



(b) Experimental result of BSPWM system (25 V/div; 4 ms/div)

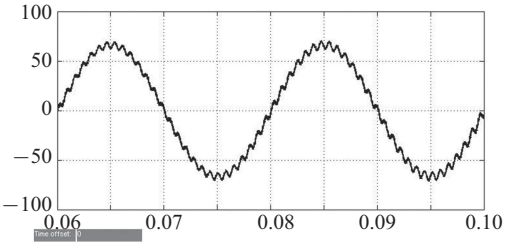


(c) Simulation result of UDFSPWM system

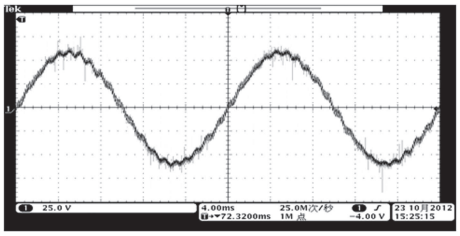


(d) Experimental result of UDFSPWM system (25 V/div; 4 ms/div)

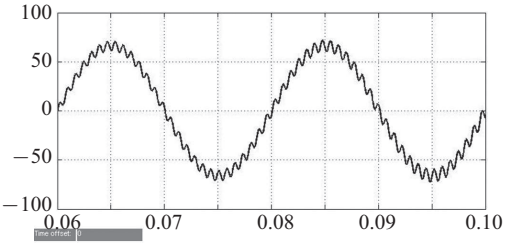
Fig. 6. Time domain waveform of v_{R} when $f_{\mathrm{s}} = 10$ kHz, $k_{\mathrm{out}} = 1$, and $k_{\mathrm{in}} = 0.9$.



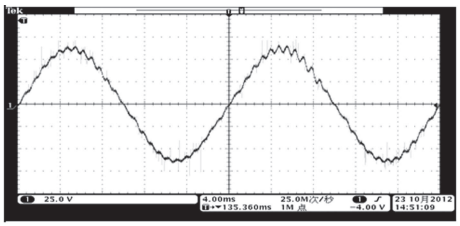
(a) Simulation result of BSPWM system



(b) Experimental result of BSPWM system (25 V/div; 4 ms/div)

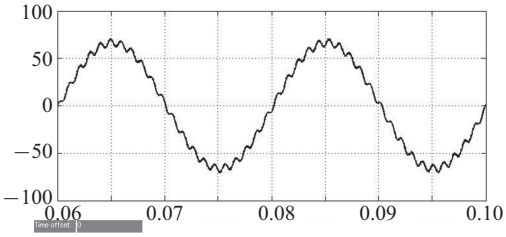


(c) Simulation result of UDFSPWM system

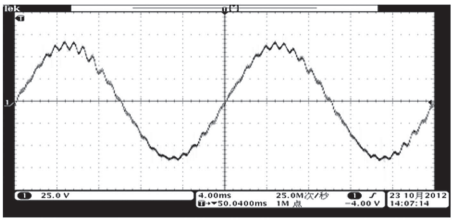


(d) Experimental result of UDFSPWM system (25 V/div; 4 ms/div)

Fig. 7. Time domain waveform of v_{R} when $f_{\mathrm{s}} = 10$ kHz, $k_{\mathrm{out}} = 1$, and $k_{\mathrm{in}} = 1$.



(a) Simulation result of UDFSPWM system



(b) Experimental result of UDFSPWM system (25 V/div; 4 ms/div)

Fig. 8. Time domain waveforms of v_{R} when $f_{\mathrm{s}} = 5$ kHz, $k_{\mathrm{out}} = 1$, and $k_{\mathrm{in}} = 0.75$.

6. Conclusions

The performances of the BSPWM and UDFSPWM strategies are compared in this paper. By establishing the discrete-time model of the system, the following conclusions are obtained. When the systems, modulated by BSPWM and UDFSPWM, have the same switching frequency, the stability boundaries of the two systems are the same. However, when the two systems have the same equivalent switching fre-

quency, the BSPWM modulated system is more stable than the UDFSPWM modulated system. In addition, a convenient method of establishing the discrete-time model for the piecewise smooth system is presented. Finally, the analytical results are confirmed by circuit simulations and experimental measurements.

The above analysis results in this paper are very helpful when analyzing the influence of the modulation method in a digitally controlled H-bridge inverter system. It will also simplify the modeling, stability analysis, and design of the piecewise smooth system.

Appendix A

$$\boldsymbol{A} = \begin{bmatrix} 0 & \dfrac{-1}{L} \\ \dfrac{1}{C} & \dfrac{-1}{RC} \end{bmatrix}, \tag{A1}$$

$$\boldsymbol{B}^{+} = \begin{bmatrix} \dfrac{1}{L} & 0 \end{bmatrix}^{\mathrm{T}}, \tag{A2}$$

$$\boldsymbol{B}^{-} = \begin{bmatrix} \dfrac{1}{L} & 0 \end{bmatrix}^{\mathrm{T}}, \tag{A3}$$

$$\boldsymbol{B}^{-} = \begin{bmatrix} 0 & 0 \end{bmatrix}^{\mathrm{T}}. \tag{A4}$$

Appendix B

The eigenvector matrix of $\boldsymbol{A}$ is denoted by $\boldsymbol{\kappa}$, and the inverse matrix of $\boldsymbol{\kappa}$ is represented by $\boldsymbol{\rho}$. The $\boldsymbol{\kappa}$ and $\boldsymbol{\rho}$ are defined, respectively, as

$$\boldsymbol{\kappa} = \begin{bmatrix} \kappa_{11} & \kappa_{12} \\ \kappa_{21} & \kappa_{22} \end{bmatrix}, \tag{B1}$$

and

$$\boldsymbol{\rho} = \boldsymbol{\kappa}^{-1} = \begin{bmatrix} \rho_{11} & \rho_{12} \\ \rho_{21} & \rho_{22} \end{bmatrix}. \tag{B2}$$

Define a function $\varepsilon(x, y, z)$ as

$$\varepsilon(x,y,z) = \kappa_{yx}\rho_{xz}, \tag{B3}$$

where the values of x, y, and z could be 1 or 2. Set ξ as

$$\boldsymbol{\xi} = \boldsymbol{A}^{-1}\boldsymbol{B}^{+}. \tag{B4}$$

Then the definition of $\sigma(x, y, z)$ and $\Gamma(x, y)$ can be expressed as

$$\sigma(x,y,z) = \left[\, \mathrm{e}^{\lambda_{A1}/x} \;\; \mathrm{e}^{\lambda_{A2}/x} \,\right] \left[\, \varepsilon(1,y,z) \;\; \varepsilon(2,y,z) \,\right]^{\mathrm{T}}, \tag{B5}$$

where the values of x, y, and z could be 1 or 2.

$$\Gamma(x,y) = \left[\, \sigma(2,x,1) \;\; \sigma(2,x,2) \,\right] \times \left[\, \left[\, \varepsilon(y,1,1) \;\; \varepsilon(y,1,2) \,\right]\boldsymbol{\xi} \;\; \left[\, \varepsilon(y,2,1) \;\; \varepsilon(y,2,2) \,\right]\boldsymbol{\xi} \,\right]^{\mathrm{T}}, \tag{B6}$$

where the values of x and y could be 1 or 2.

Appendix C

F_0, F_1, and F_2 can be described, respectively, as

$$F_0 = k_{\mathrm{sat}}((\Lambda_2\sigma(1,1,2) - \Lambda_1\sigma(1,2,2))k_{\mathrm{in}} + (\Lambda_1\sigma(1,2,1) - \Lambda_2\sigma(1,1,1))k_{\mathrm{in}}k_{\mathrm{out}}), \tag{C1}$$

$$F_1 = \sigma(1,1,1)\sigma(1,2,2) - \sigma(1,1,2)\sigma(1,2,1) + k_{\mathrm{sat}}k_{\mathrm{in}}(\Lambda_1 + \Lambda_2 k_{\mathrm{out}}), \tag{C2}$$

$$F_0 = \sigma(1,1,1) + \sigma(1,2,2), \tag{C3}$$

$$\gamma_1 = 2(1 - \sigma(1,1,1)\sigma(1,2,2) + \sigma(1,1,2)\sigma(1,2,1)), \tag{C4}$$

$$\gamma_2 = k_{\mathrm{sat}}(\sigma(1,1,1) + \sigma(1,2,2))(\Lambda_1\sigma(1,2,2) - \Lambda_2\sigma(1,1,2)) + 2\Lambda_1, \tag{C5}$$

$$\gamma_2 = k_{\mathrm{sat}}(\sigma(1,1,1) + \sigma(1,2,2))(\Lambda_2\sigma(1,1,1) - \Lambda_1\sigma(1,2,1)) + 2\Lambda_2. \tag{C6}$$

References

[1] Blaabjerg F, Teodorescu R, Liserre M and Timbus A V 2006 *IEEE Trans. Ind. Electron.* **53** 1398

[2] Kjaer S B, Pedersen J K and Blaabjerg F 2005 *IEEE Trans. Ind. Electron.* **41** 1292

[3] Peterchev A V and Sanders S R 2003 *IEEE Trans . Power Electron.* **18** 301

[4] Xiao H and Xie S 2010 *IEEE Trans. Electromagn. Compat.* **52** 902

[5] Zang C, Pei Z J, He J J, Ting G, Zhu J and Sun W 2009 *Proceedings of PEDS 2009*, November 2–5, 2009, Wuhan, China, p. 1439

[6] Townsend C, Summers T J and Betz R E 2010 *Proceeding of* 36*th Annual Conference on IEEE Industrial Electronics Society*, November 7–10, 2010, Glendale, AZ, p. 2019

[7] Townsend C, Summers T J and Betz R E 2010 *Proceeding of* 36*th Annual Conference on IEEE Industrial Electronics Society*, November 7–10, 2010, Glendale, AZ, p. 2025

[8] Hooman D, Nayar C V and Chang L 2003 *Proceedings of ISIE*, January 9–11, 2003, Rio de Janeiro, Brazil, p. 985

[9] Venkatasubramanian D, Natarajan S P and Shanthi B 2012 *Int. J. Comput. Appl.* **49** 26

[10] Zhang Z C and Ooi B T 1993 *IEEE Trans. Ind. Electron.* **8** 250

[11] Zhu J W and Gong C Y2004 *Power Electron* **38** 25 (in Chinese)

[12] Zhou J H, Yang Z and Su Y M 2005 *Electric Drive* **35** 23

[13] Lei B, Xiao G C, Wu X L and Qi Y R 2011 *Acta Phys. Sin.* **60** 090501 (in Chinese)

[14] Lei B, Xiao G C and Wu X L 2012 *Acta Phys. Sin.* **61** 090501 (in Chinese)

[15] Lu W G, Zhou L W and Luo Q M 2007 *Chin. Phys.* **16** 3256

[16] Zhou G H, Xu J P, Bao B C, Zhang F and Liu X S 2010 *Chin. Phys. Lett.* **27** 090504

[17] Tse C 2003 *Complex Behavior in Switching Power Converters* (New York: Boca Raton, CRC) p. 59